

Micromechanics of smooth adhesive organs in stick insects: pads are mechanically anisotropic and softer towards the adhesive surface

Ingo Scholz · Werner Baumgartner ·
Walter Federle

Received: 17 October 2007 / Revised: 11 December 2007 / Accepted: 4 January 2008 / Published online: 25 January 2008
© Springer-Verlag 2008

Abstract Animals have evolved adhesive structures on their legs to cling to the substrate during locomotion. Here we characterise the ultrastructure and mechanical properties of adhesive pads in *Carausius morosus* (Phasmatodea) using atomic force microscopy (AFM) as well as transmission and scanning electron microscopy (TEM, SEM). The smooth adhesive arolium has a soft cuticle consisting of principal rods, which branch into finer fibres near the surface. Indentation experiments showed that the pad material consists of distinct layers with different mechanical properties. The 100–300 nm thick outermost layer consisting of the cuticulin envelope and the epicuticle is extremely soft and resilient (mean effective Young's modulus 12 kPa), while the subjacent procuticle is a much stiffer material (mean effective Young's modulus 625 kPa). AFM contact mode imaging revealed that the cuticle is mechanically anisotropic, which can be explained by its fibrillar inner structure. We propose that the described layered structure of smooth adhesive pads, consisting of materials decreasing in stiffness towards the outer surface, represents a superior design to conform and adhere to substrates with roughnesses at different length scales. This design principle could be easily implemented in technical adhesives, and thus has a potential to inspire biomimetic applications.

Keywords *Carausius morosus* · Tribology · Microindentation · Insect cuticle · AFM

Introduction

Many insects possess specialised attachment organs on their legs, which enable them to climb and run upside down on various substrates. Some species are not only capable of resisting extreme pull-off and shear forces equivalent to more than 100 times their own body weight (Eisner and Aneshansley 2000; Federle et al. 2000), but they can also run rapidly. The detailed underlying mechanisms of this impressive performance are still unclear, and some may be based on the detailed ultrastructure and physical properties of adhesive organs.

Adhesive structures in arthropods and vertebrates have been classified as “smooth” pads with a soft cuticle and “hairy” systems, i.e. pads densely covered with microscopic adhesive setae. Despite their microstructural similarity, adhesive pads in different insect orders are found at different positions of the leg, providing evidence for multiple evolutionary origins of these organs (Beutel and Gorb 2001; Beutel and Gorb 2006). They can be located on different tarsal segments (e.g. euplantulae) and/or the pretarsus (e.g. as pulvilli or arolium). The cuticle of smooth pads differs structurally from typical hard exoskeleton cuticle and from the soft and flexible cuticle found in joints and extensible body parts (Reynolds 1975; Vincent 1981) in that its rod-like fibres are not arranged parallel to the surface, but are oriented at some angle to it.

The arolium is probably an autapomorphy of the Neoptera (Beutel and Gorb 2006) and is homologous in the Dictyoptera, Phasmatodea and Orthoptera. Its morphology differs from the derived, unfoldable arolia occurring in the

I. Scholz · W. Baumgartner
Department of Cellular Neurobiology, Institute of Biology 2,
RWTH-Aachen, Kopernikusstr. 16, 52068 Aachen, Germany

W. Federle (✉)
Department of Zoology, University of Cambridge,
Downing Street, Cambridge CB23EJ, UK
e-mail: wf222@cam.ac.uk

Hymenoptera, Mecoptera and Trichoptera (Holway 1935; Snodgrass 1956). The basic non-unfoldable type of arolium has been investigated morphologically by several authors (Beutel and Gorb 2001; Kendall 1970; Roth and Willis 1952; Slifer 1950), using light microscopy but its mechanical properties have remained unstudied. Here we characterise the morphology, ultrastructure and mechanical properties of the arolium in *Carausius morosus* by using freeze-fracture SEM, TEM, confocal laser scanning microscopy (CLSM) and atomic force microscopy (AFM). We demonstrate that CLSM using cuticular autofluorescence is a suitable method for visualising the orientation of fibres within adhesive pad cuticle.

Previous studies investigating the mechanical properties of smooth adhesive pads in insects either made conclusions from the load–displacement behaviour of whole pads (Gorb et al. 2000; Jiao et al. 2000) or employed microindenters with spherical tips with radii $>32\ \mu\text{m}$ (Perez Goodwyn et al. 2006). In this study we characterise the micromechanics of the arolium using AFM. The advantage of this technique in comparison to previous approaches is that it allows the material properties to be measured with high spatial resolution, due to the much smaller size of the pyramidal AFM indenter. This makes it possible to determine the actual material properties of the specialised cuticle independent of the mechanical arrangement of the adhesive pad structure.

The aim of our study is to (1) characterise the morphology and ultrastructure of the arolium in *C. morosus* and (2) investigate its mechanical properties with high spatial resolution.

Materials and methods

Study animals

Adult female stick insects (*C. morosus*; body weight: $762 \pm 154\ \text{mg}$, length: $79.0 \pm 5.7\ \text{mm}$; mean \pm standard deviation, $n = 17$) were taken from our laboratory colony at the RWTH Aachen and were used for the experiments.

Confocal laser scanning microscopy (CLSM)

Adult stick insects ($n = 2$) were cooled down at 4°C for 10 min and decapitated. The arolia of all six feet were carefully cut from the tarsus using a razor blade, embedded in glycerine (80% in distilled water) on a microscope slide and covered with a cover slip. Observations were made immediately after preparation under a confocal laser-scanning microscope (Leica TCS SP2; Leica Microsystems, Wetzlar, Germany). Using two lasers for excitation at

405 nm and 543 nm wavelength, single projections and serial optical sections of different thicknesses were generated with a $25\times$ objective (Glycerine) and a $63\times$ objective (Glycerine). The images were stored in a 512×512 , $1,024 \times 1,024$ or $1,280 \times 1,280$ pixel format. The images presented here were obtained by combining a 405 nm and a 543 nm laser, which yielded the best contrast and image quality.

Scanning electron microscopy (SEM)

External and internal morphology of the insect tarsi were obtained using different SEM techniques: (I) Overview images of the surface and external parts of the tarsus were obtained using fixed whole insects, (II) freeze fractures of the tarsi were used to investigate internal structures.

- (I) Adult insects ($n = 2$) were shock frozen in a bath of melting pure ethanol cooled in liquid nitrogen at about -114°C , transferred into -80°C cold ethanol containing 0.5% glutardialdehyde (GA; Merck, Darmstadt, Germany) and stored at -80°C for 48 h. Afterwards GA concentration and temperature were gradually increased: 2% GA at -80°C for 48 h, 4% GA at -20°C for 96 h and 10% GA at 4°C for 120 h. After washing in hexamethyl-disilazane (HMDS; Merck) and air drying, the specimens were gold coated with a sputter coater (Humme, Technics Inc., Alexandria, USA). The thickness of the gold coat was less than 2 nm. Observations were made with a Cambridge Stereoscan 604 scanning electron microscope (Cambridge Instruments, UK).
- (II) Frozen insect pads (9 arolia of 3 adult individuals) were fractured using a razor blade immersed in pure ethanol in a petri dish cooled down in a Styrofoam box with dry ice at about -74°C . The fractured samples were treated like whole insects, as described above.

Transmission electron microscopy (TEM) and light microscopy

For transmission electron microscopy (TEM), samples (6 arolia of 2 adult individuals) were shock frozen in pure ethanol at about -114°C (see above). Fixation was performed in 0.5% GA in pure ethanol at -80°C for 48 h, then transferred into 2% GA at -20°C for 96 h and finally stored at 4°C in a 4% GA for further 72 h. The tissues were postfixed for 1 h in 1% osmium tetroxide (Fluka, Switzerland) in phosphate buffered saline (PBS; Appli-Chem, Germany), washed in distilled water (3 times

for 15 min), and stained for 1 h with 2% uranyl acetate solution in ethanol (Merck) in a dark environment. Afterwards the tissue was washed in ethanol (70, 80, 90, 96 and 100%, each for 15 min), dehydrated two times for 30 min in propylene oxide (SERVA, Germany) and stored for 16 h in a mixture of propylene oxide and epoxy resin (Epon; SERVA). After washing in Epon (two times for 2 h) the samples were embedded and polymerised for 48 h at 57°C.

Ultra thin sections were made with a Reichert OmU3 ultramicrotome (C. Reichert AG, Austria) and placed on 200 mesh (200 division bars on 25.4 mm) nickel grids (Plano GmbH, Germany). Observations were made with a Zeiss EM 10C transmission electron microscope (Zeiss, Germany).

For light microscopy, semi-thin sections of the arolium were prepared by fixing and dehydrating samples as for SEM (see above). The dry samples were then embedded for 16 h in the mixture of propylene oxide and Epon and further treated like the TEM samples. Polymerised resin blocks were sectioned serially with 1 µm thickness. Sections were attached to albuminised glass slides, stained with methylene blue at 60°C and washed with H₂O.

Atomic force microscopy (AFM)

All AFM measurements were performed at room temperature with a Veeco Dimension III scanning probe microscope and a NanoScope III Bioscope controller (Veeco, Woodbury, NY, USA). To reduce vibrations, the AFM was held by elastic bands in an acoustically isolated box. Indentation measurements and imaging were performed in AFM contact mode. We used silicon nitride cantilevers with spring constants of 0.01 and 0.03 N/m (Type MLCT, Veeco Instruments). The cantilever tips had a four-sided pyramidal shape (corresponding to a Vickers-type indenter) with a centreline-to-face tip angle of 35°. General principles of AFM measurements in living biological structures are given by Morris et al. (1999). Data were analysed with custom-made software using MATLAB (The Mathworks, USA).

A stick insect was enclosed in an aluminium tube (6 mm inner diameter, 100 mm length) on which a thin copper-wire (1 mm × 60 mm) was bonded to the side. The wire overlapped the tube by about 20 mm. The dorsal side of one foreleg tarsus (including the 5th tarsal segment and the pretarsus) was fixed to this copper wire using melted modelling-wax. The claw tips of the legs were cut off, so they could not get in contact with the cantilever. The arolium was then placed directly underneath the AFM cantilever. To prevent desiccation and minimise the effects of capillary forces, measurements were carried out

underwater in insect ringer (10.4 g NaCl, 0.32 g KCl, 0.48 g CaCl₂, 0.32 g NaHCO₃ in 1 l pure water). The position of the pad was controlled via a video camera from underneath. The set-up was moved with a home-built XYZ micromanipulator.

During the measurements, the insect was anaesthetised by a gentle flow of CO₂ applied through the end of the metal tube. The flow rate did not interfere with the measurements and did not cause any damage to the stick insects. All insects recovered after the experiments and were returned to the colony. Two types of measurements were carried out using this set-up: (a) surface scanning of the arolium and (b) indentation at different points on the arolium.

Surface imaging of the arolium

The surface of the adhesive pad was scanned to obtain information on its structure and its mechanical properties *in vivo*. Because of the anisotropy of friction forces previously reported for other insects with smooth pads (see “Introduction”), the surface was scanned in different directions. It must be pointed out that, during imaging, the AFM scans the sample in only one direction. We therefore scanned the arolium in four different ways: (1) longitudinally, from proximal to distal (“trace”), (2) longitudinally, from distal to proximal (“retrace”), (3) transversely, from left to right (“trace”) and (4) transversely, from right to left (“retrace”) (see Fig. 5, scanning directions are indicated by black arrows). The scanning direction was changed in random order to exclude possible influences from the previous scan.

Because of the 13°-inclination of the cantilever towards the surface, scanning movements along the axis of the cantilever or perpendicular to it could lead to different results. Therefore we oriented the insect tarsus at 45° to the axis of the cantilever so that both the longitudinal and the transverse scans were performed at a 45° angle to the axis of the cantilever. This ensured equal conditions for each of the four scans.

The scan size for the surface scanning of the pad was 30 × 30 µm at a scan rate of 60 µm s⁻¹ (1 Hz). The applied force of the cantilever was about 6 nN. Three arolia of two adult stick insects were used for surface imaging.

The following surface profile parameters were obtained: (1) the roughness average (R_a), which is the average of the absolute values of the profile height deviations from the centreline over the evaluation length, in our case over the whole scanned area. (2) The maximum roughness depth (R_{max}), which is the value of the distance between the maximum peak to lowest valley of the profile. (3) The mean spacing of longitudinal ridges (S), which describes the mean distance between peaks for a transverse scan.

R_a and R_{max} were calculated with the NanoScope Software 6.13 (Veeco Digital Instruments, Woodbury, NY, USA). S was calculated from 15 transverse line scans per image (Fig. 5) at regular intervals of 2 μm .

Indentation measurements

Measurements of the effective Young's modulus (i.e. the elastic modulus) of the adhesive pad materials were performed with a z -drive amplitude of 1,000 nm and at rates of 1 or 2 Hz (corresponding to z -velocities of 2 and 4 $\mu\text{m s}^{-1}$, respectively). Two different measurements were performed:

- (A) Force–distance curves were recorded in the centre of the adhesive contact zone (2 arolia from 2 individuals, 10 positions per arolium, each with 20 consecutive indentations). The indentation positions were randomly chosen within a small area of about $10 \times 10 \mu\text{m}$, with a distance of at least 1 μm between indentation points. The time between consecutive indentations at the same point was 1 or 0.5 s (for rates of 1 or 2 Hz, respectively). The indentation data were used to calculate the material properties of the adhesive cuticle.
- (B) To assess the variation of the thickness of the soft epicuticle layer, a series of additional indentations were performed on the medial distal side of the arolium contact zone in a $14 \times 14 \mu\text{m}$ area, with a grid spacing of 2 μm (resulting in a total of 64 points, each with 20 consecutive indentations).

For determination of the elastic modulus, we analysed the indentation force–distance curves. Measurements affected by mechanical vibrations, instability and movements of the live stick insect were excluded from the analysis. As unloading curves often exhibited irregular adhesion peaks due to tip-sample interactions, we used the loading curves for technical simplicity. This is also justified due to the absence of plastic deformation (Oliver and Pharr 2004).

For an ideal indentation of a homogeneous flat material the force–indentation relation is a power law (Oliver and Pharr 2004):

$$F = \alpha z_i^m \quad (1)$$

where F is the applied force, α a material parameter directly related to the effective Young's modulus (see below), z_i the indentation depth and m an exponent representing the geometry of the indenter. An ideal flat punch without any tip or side effects would yield $m = 1$ whereas an ideal pyramidal or conical indenter would yield $m = 2$, if tip rounding and side effects can be neglected (Attaf 2004; Malzbender et al. 2000). In our case we investigated a rather soft material with moderate indentation depth,

which was much larger than the tip radius. Thus the simplifying approximation of $m = 2$ is valid, and it was found to be consistent with our data.

When force–distance curves are measured in the AFM, neither the indentation depth nor the force is directly accessible, as we measure the z -position and the deflection of the cantilever. The force however is directly proportional to the cantilever deflection ($F = k d$). The indentation depth equals the z -displacement after the point of contact (z_0) minus the deflection ($z_i = z - z_0 - d$). The force equilibrium at the tip is

$$F = kd = \alpha(z - z_0 - d)^2 \quad (2)$$

Solving the quadratic equation above for the deflection d yields

$$d = (z - z_0) + \frac{k}{2\alpha} - \sqrt{\left((z - z_0) + \frac{k}{2\alpha}\right)^2 - (z - z_0)^2} \quad (3)$$

For the analysis of force–distance curves consisting of two distinct parts representing an outer layer (thickness h) of material 1 and an inner layer of material 2 with different elastic moduli (Fig. 6), the superposition was modelled as:

$$d_{\text{total}} = d_1 + d_2 = \begin{cases} d([z - z_0], \alpha_1) + 0 & \text{if } z_1 < h \\ d(h, \alpha_1) + d([z - z_0 - h], \alpha_2) & \text{if } z_1 \geq h \end{cases} \quad (4)$$

The force–distance curves were fitted using this equation with the free parameters $\alpha_{1/2}$, z_0 and h being optimised by a Levenberg–Marquart least square fitting procedure.

For a homogeneous elastic material and a pyramidal indenter, the fitted parameter α relates to the effective Young's modulus as (Oliver and Pharr 2004)

$$\frac{\partial F}{\partial z_i} \cong \frac{2}{\sqrt{\pi}} 2z_i \tan(\theta) E_{\text{eff}} = 2\alpha z_i \Rightarrow E_{\text{eff}} \cong \frac{\sqrt{\pi} \alpha}{2 \tan(\theta)} \quad (5)$$

where θ is the tip angle of the indenter and E_{eff} is the effective Young's modulus given as

$$\frac{1}{E_{\text{eff}}} = \frac{1 - \nu^2}{E} + \frac{1 - \nu_0^2}{E_0} \quad (6)$$

E and ν are the Young's modulus and the Poisson's ratio of the sample, respectively; E_0 and ν_0 are the same parameters for the indenter. As the indenter material (i.e. silicon nitride) is much harder than the pad material, Eq. 6 can be simplified yielding

$$E_{\text{eff}} = \frac{E}{1 - \nu^2} \quad (7)$$

Thus, if the Poisson's ratio is known, E can be calculated. As its exact value is unknown for the cuticle investigated, however, we will only report the effective Young's modulus. All measurements are reported as mean values with standard deviations.

Results

General morphology

The tarsus and the adhesive organ of *C. morosus* show the same features as described for representatives of the Blattodea and Orthoptera (Beutel and Gorb 2001; Slifer 1950). The tarsus is divided into five segments, and the pretarsal arolium is located in between the claws. The adhesive contact zone of the arolium is kidney-shaped and reveals a smooth surface with no visible structures in light microscopy and low magnification SEM images (Fig. 1a). It is surrounded by sclerotised pretarsal structures, the planta on the proximal side and the manubrium on the dorsal side. The overall adhesive contact area of the arolium of a foreleg in adult stick insects had an average size of $793 \mu\text{m}$ ($\pm 109 \mu\text{m}$) \times $320 \mu\text{m}$ ($\pm 51 \mu\text{m}$) (width \times length; mean \pm SD, $n = 11$). There were no differences in the general structure between fore, middle and hind legs. Higher magnification revealed fine grooves running along the longitudinal axis of the tarsus (Fig. 1b).

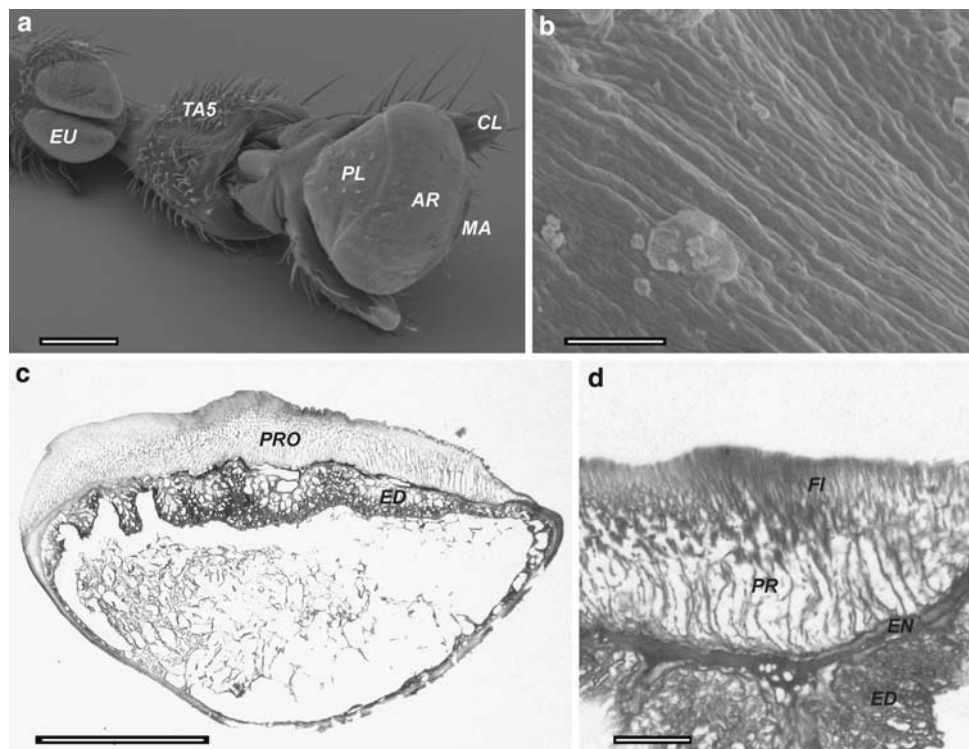
Inner morphology

Figure 1c, d shows semithin cross-sections, Fig. 2 SEM freeze fractures and Fig. 3 TEM images of the arolium and its adhesive cuticle. The fibrous inner structure of the

arolium cuticle in *C. morosus* is similar to that of other smooth pads [e.g. *Melanoplus differentialis* (Slifer 1950), *Tettigonia viridissima* (Gorb et al. 2000)]. The thin, outermost layer is the electron-dense cuticulin layer of the epicuticle. In the TEM images it appears dark and non-structured with a thickness of 10–20 nm (average of 16 ± 8 nm 17 measurements from 3 samples) (Fig. 3b). The subjacent inner epicuticle layer appears brighter in the TEM images but is also amorphous (Fig. 3a, b). The thickness of this layer varied between 100 nm and 400 nm (mean 208 ± 103 nm). This layer is traversed by fine electron-dense lines of 15–25 nm width, which can be seen in the TEM images to consist of filamentous structures of only ca. 6–7 nm width (Fig. 3b, c). By analogy with similar structures found in the cuticle of other insects we conclude that these structures represent pore canals containing numerous filaments (Locke 1961).

Underneath the inner epicuticle, there is a thick procuticle (Figs. 1c, d, 2b, c and 3a). It contains principal (first order) cuticular rods, which are oriented almost perpendicularly to the surface (Figs. 1c, d, 2b, c). The length of these rods ranged from 44 to 74 μm (mean $64.8 \pm 9.1 \mu\text{m}$; $n = 26$), and their diameter from 0.89 to 3.38 μm (mean $1.65 \pm 0.75 \mu\text{m}$; $n = 30$). In the outer 2–4 μm of the procuticle, the principal rods ramify into finer (second order) branches (Figs. 1c, d, 2b). Branching of fibres close to the surface has also been reported from smooth adhesive pads of other insects (Beutel and Gorb 2001; Gorb et al. 2000; Kendall 1970; Slifer 1950).

Fig. 1 **a** SEM image of the tarsus and the adhesive structure (arolium) of *C. morosus*. **b** SEM image of the ultrastructure of the arolium. **c, d** semi-thin, transverse section of the arolium, light microscopy. *AR* arolium, *CL* claw, *ED* epidermis, *EN* endocuticle, *EU* euplantulae, *FI* fine fibres, *MA* manubrium, *PRO* procuticle, *PL* planta, *PR* principal rods, *TA5* fifth tarsal segment. Scale bars: **a** 400 μm , **b** 4 μm , **c** 200 μm , **d** 20 μm



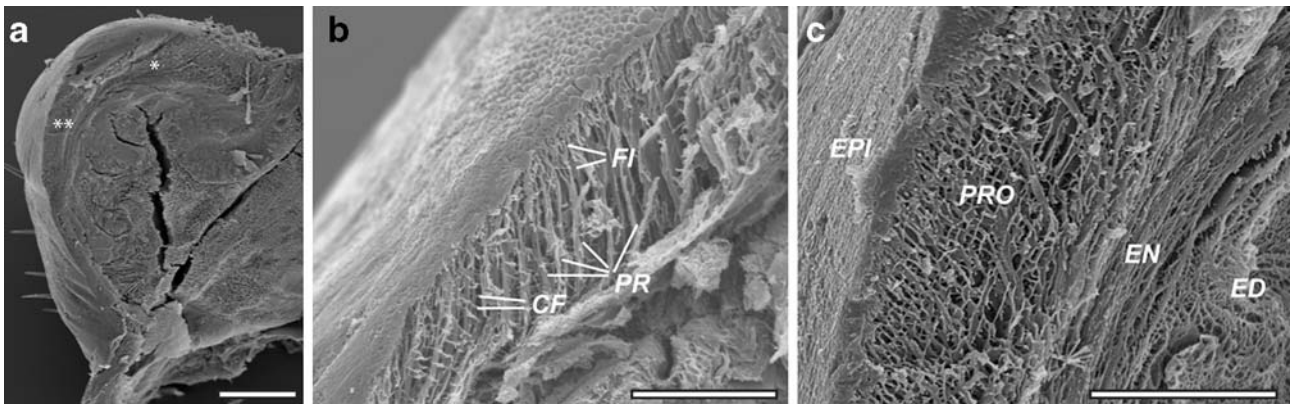


Fig. 2 Ultrastructure of the arolium cuticle, freeze fractures. **a** Overview of pad. The white asterisks indicate the position of detail views **b** (*) and **c** (**). **b** Principal rods (*PR*) branching into fine fibres (*FI*), and connecting filaments (*CF*). **c** Layered construction of the

arolium cuticle. *ED* epidermis, *EN* endocuticle, *EPI* epicuticle, *PR* principal rods, *PRO* procuticle with rods. Scale bars: **a** 100 μm , **b**, **c** 50 μm

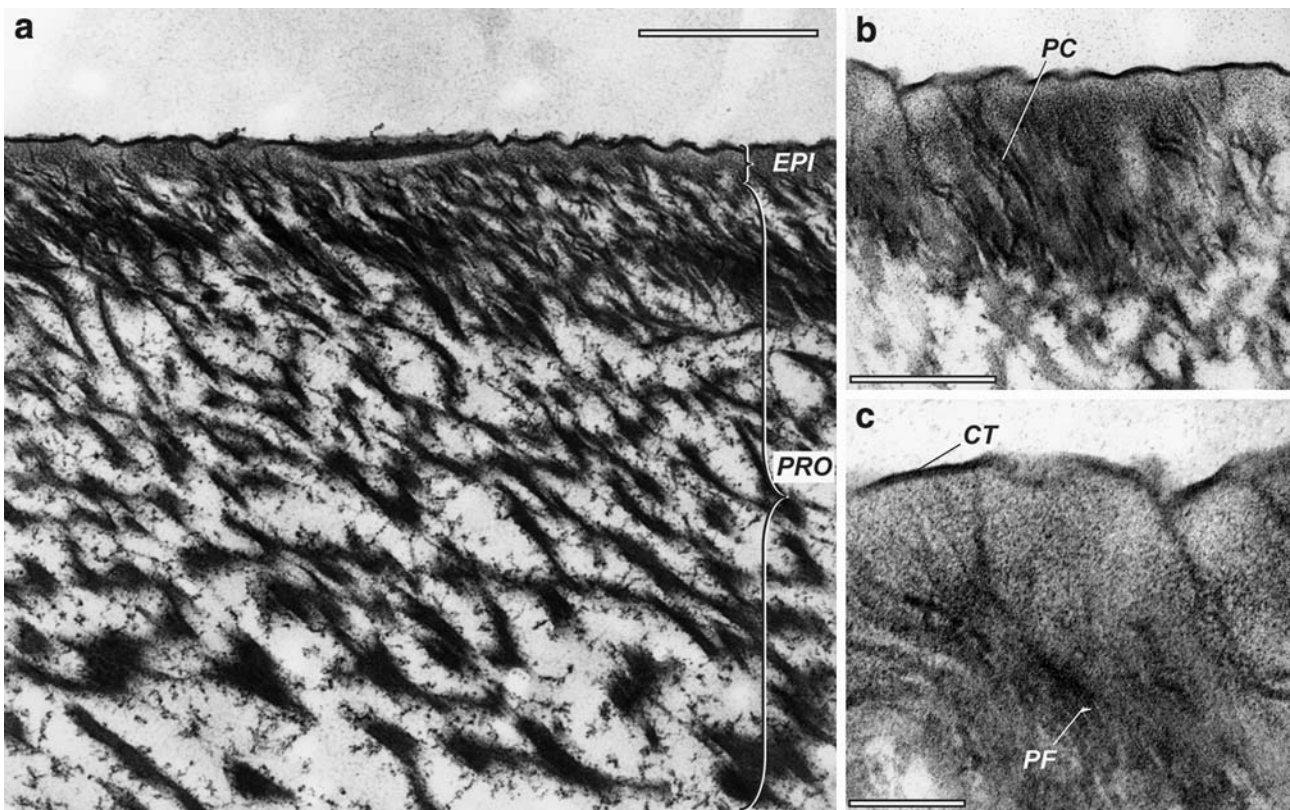


Fig. 3 **a** Section of adhesive arolium cuticle in *C. morosus*, TEM image. The cuticle fibres close to the surface are branches of the principal rods from the deeper procuticle. **b** and **c**: Details of

epicuticle with pore canals and cuticulin layer. *EPI* epicuticle, *PRO* procuticle, *CT* cuticulin layer, *PC* pore canals, *PF* pore canal filaments. Scale bars: **a** 1 μm , **b** 500 nm, **c** 200 nm

Using confocal microscopy, we found that the principal rods are arranged over the contact zone of the arolium in a regular pattern. They are aligned in rows running from the proximal to the distal side of the contact zone (Fig. 4). At the proximal end of the arolium contact zone (Fig. 4) the rods are seen in cross-section (i.e. parallel to the optical axis). Inside the contact zone, the rods are oriented distally,

i.e. they stand at an angle to the optical axis (this can also be seen in Fig. 2). The superimposed image of several rods seen using CLSM gives the impression of thick and long “hyper-rods”, running longitudinally through the pad contact zone.

The transverse spacing between the principal fibres and thus between the rows they form is 1.5–5.5 μm (mean

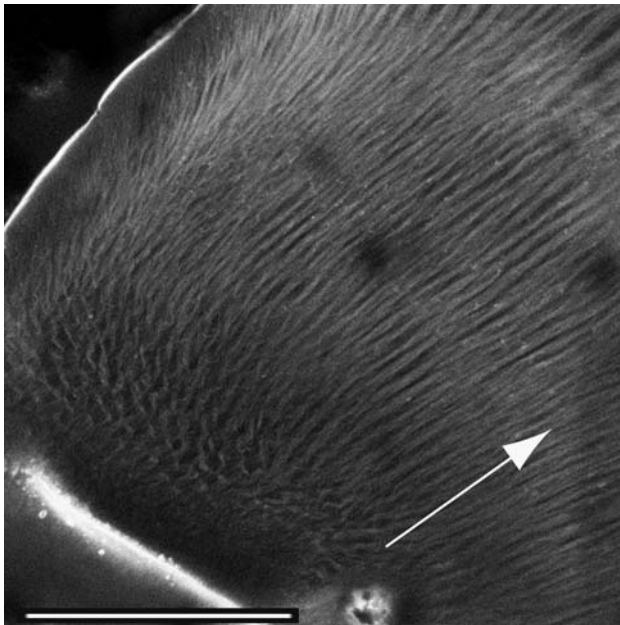


Fig. 4 Longitudinal rows of principal rods in the arolium cuticle, ventral view of the contact zone CLSM (excitation wavelength: 405 and 543 nm). White arrow indicates distal direction of the arolium. Scale bar: 100 μm

4.05 ± 1.25 ; $n = 15$) (Figs. 1d, 4). Underneath the layer of the principal rods lies the endocuticle. It adjoins to the epidermis and appears unstructured (Fig. 1d). The space underneath the epidermis is filled with haemolymph. Because of the preparation and drying of the tissue, the interior part of the arolium appears sponge-like in the freeze-fracture SEMs (Fig. 2a).

Atomic force microscopy (AFM)

Surface imaging

In the first experiment, the surface of an adhesive pad was scanned in longitudinal direction (Fig. 5a, b). The two images obtained were in all cases very similar. Only a small shift in x - and y -direction of the whole image could be seen due to a deficient synchronisation of the AFM scanner. “Trace” and “retrace” height profiles at the same positions were very similar in terms of their maximum roughness depth (Image R_{max}), the average roughness (Image R_{a}) and the mean spacing of longitudinal ridges (S). These data are summarised in Table 1.

The difference between trace and retrace scans was also negligible when the pad was scanned in transverse direction (Fig. 5c, d; Table 1). However, the height profile was considerably different from that measured with longitudinal scans (see Fig. 5a vs. c, and b vs. d). The

topography obtained by the longitudinal scanning was much shallower than the corresponding “transverse” profile. However, the spacing of longitudinal ridges (S) remained similar.

Indentation measurements

The AFM force–distance curves of the whole arolium showed a characteristic shape (Fig. 6). When the tip of the cantilever made contact with the pad, it showed only a very small deflection, indicating a very low effective Young’s modulus for the outermost layer of ca. 200 nm thickness (Section 1). From that indentation depth onwards, the deflection increased more strongly, indicating the presence of a harder material. This layer (Section 2) was thicker than the z -range of the AFM scanner (i.e. $>2 \mu\text{m}$).

The indentation curves did not show a simple exponential shape as expected for the indentation of a homogeneous material, but consisted of two distinct parts. Hence the two curve sections were analysed separately, to fit Eq. 3 as indicated in Fig. 6. The transition point was determined by the fitting algorithm.

From the fitted curves, values of α and the effective Young’s modulus (E_{eff}) were calculated according to Eq. 5. For the outer layer, we obtained a thickness of $213 \pm 56 \text{ nm}$ and an effective elastic modulus of $12 \pm 3 \text{ kPa}$ (mean \pm SD; $n = 204$ measurements from 17 positions on three arolia from different stick insects; range 92–323 nm and 8–26 kPa), for the inner layer, however, a much higher value of $625 \pm 291 \text{ kPa}$ was found (mean \pm SD; $n = 204$; range 188–1,244 kPa). Because the E_{eff} of the thin outer layer was less than 5% of that of the inner layer, its presence had only a minimal influence on the indentation of the thick inner cuticle and was therefore neglected. The good correspondence between data and fit (Fig. 6) indicates that this approximation is justified.

Consecutive indentations at the same point did not reveal any significant changes, indicating that the indentation of the pad material was not influenced by viscous effects or plastic deformation. This was also confirmed by scans of the indented area, which showed no visible effects of the previous indentations.

(B) Our indentation measurements indicate a regular pattern of the thickness of the epicuticle layer. As the thickness of the epicuticle was derived from the force–distance curves (cf. Fig. 6), the data shown in Fig. 7 illustrate the thickness of the epicuticle independent of the topography of the adhesive surface. The figure suggests that there are lines of thicker epicuticle running along the proximal–distal axis of the arolium, with spacing

Fig. 5 Topographic AFM images of the arolium in *C. morosus*. All images show the same area of the pad, but under different scan directions, which are indicated by *black arrows*. The distal direction (i.e. to the leg tip) in every scan is toward the top of the images

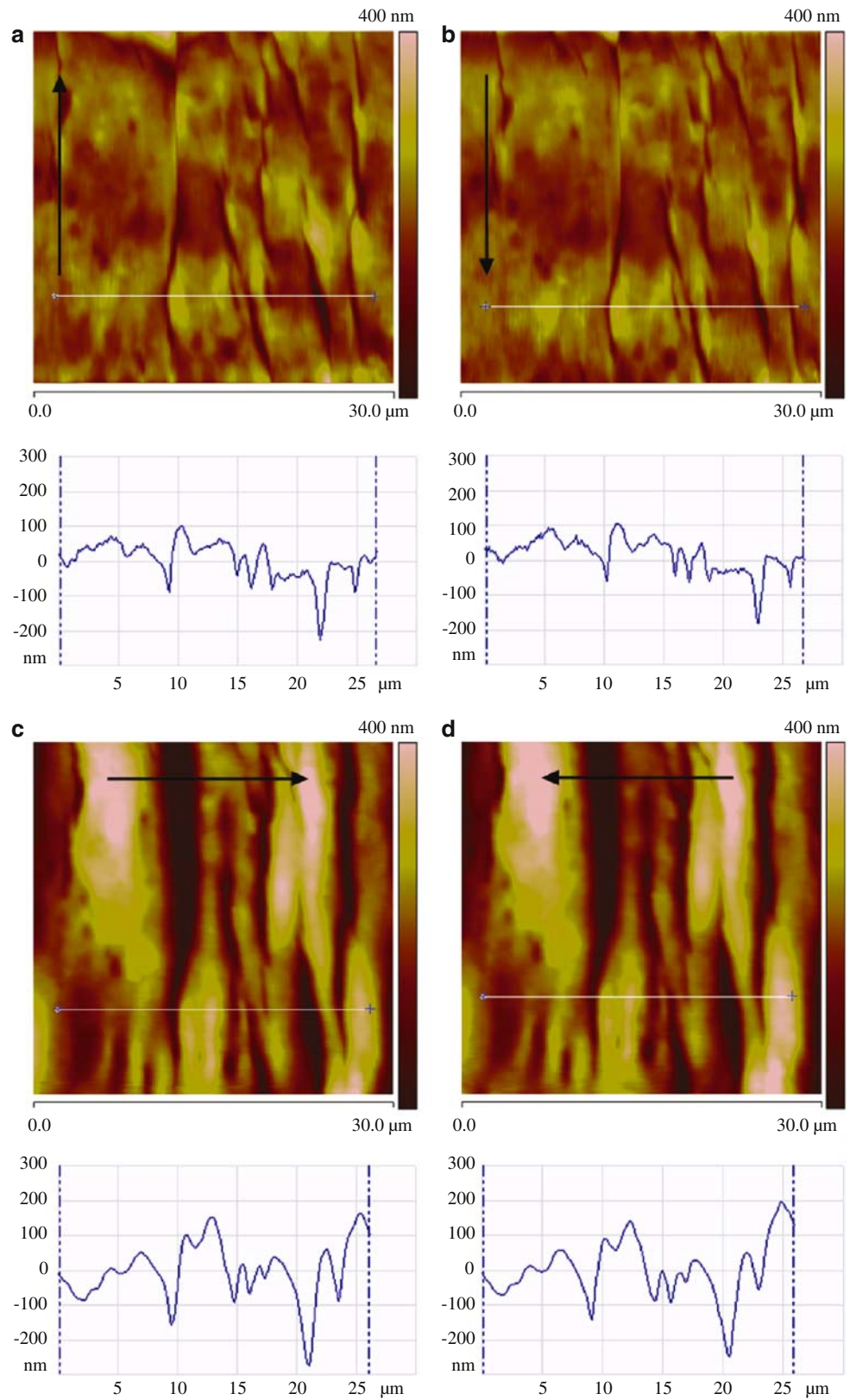


Table 1 Surface profile parameters of the AFM scans shown in Fig. 5

	Longitudinal		Transverse	
	Trace	Retrace	Trace	Retrace
R_{\max} (nm)	423	349	760	734
R_a (nm)	31.0	29.7	80.3	82.4
S (μm)	3.38 ± 1.19	3.13 ± 1.11	3.59 ± 1.50	3.35 ± 1.06

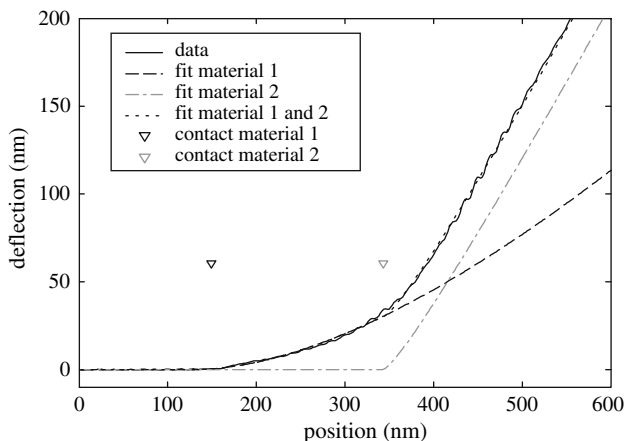


Fig. 6 Force–distance curve of indentation experiment on arolium of *C. morosus*. The indentation curve shows two characteristic segments, indicating a change of material properties. The black triangle denotes the point where the cantilever made contact with the pad (contact material 1). The point where the slope of the curve changes due to the interaction of the tip with the harder pad material is indicated by the grey triangle (contact material 2). From the fits of the first (fit material 1) and second (fit material 2) part of the curve results the final fit (fit material 1 and 2) of the whole curve

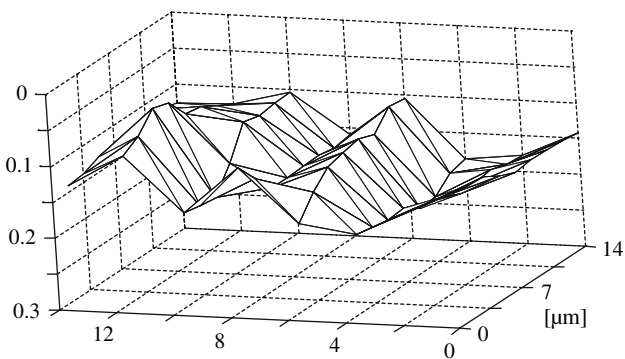


Fig. 7 Thickness of the epicuticle as estimated from the AFM force–distance curves. Measurements were performed in a $14 \times 14 \mu\text{m}$ area with a grid spacing of $2 \mu\text{m}$. Zero on the z-axis corresponds to the arolium surface

comparable to the longitudinal ridges found in the AFM topography (Fig. 5) and the rows of principal rods visible in the CLSM images (Fig. 4).

Discussion

Morphology

The arolium in stick insects (*C. morosus*) represents an adhesive pad structure of the “smooth” type. Even though its adhesive cuticle looks smooth macroscopically, it is characterised by a regular pattern of surface corrugations. Similar surface morphologies have been reported from smooth adhesive pads in a number of insect taxa (Beutel and Gorb 2001). In contrast to other insects with hexagonal or transverse surface patterns, the structure in *C. morosus* mainly consists of longitudinal ridges. The diversity of surface microstructures among smooth adhesive pads of insects suggests that it is mainly their presence rather than their detailed geometry that is functionally important. We think that the main function of the surface ridges and grooves is to allow rapid spreading and drainage of liquid secretion in order to facilitate contact formation (Barnes 1999; Federle et al. 2006; Persson 2007). While fluid films help to increase adhesion and maximise contact area on rough substrates, they will also lubricate the pad contact zone and reduce friction (Drechsler and Federle 2006). When pads make contact to a substrate during locomotion, excessive fluid in the contact zone will be drained much faster through the surface channels than it would if unstructured surfaces were squeezed together. A second possible advantage of narrow surface channels may be that they help to recover fluid during pad detachment via surface tension forces.

Our findings on the structure of the arolium in *C. morosus* are consistent with information available on the arolium of locusts (Kendall 1970), grasshoppers (Slifer 1950) and cockroaches (Arnold 1974; Roth and Willis 1952). As in these species, the arolium cuticle of *C. morosus* is characterised by a loose fibrous structure of perpendicular rods that branch into finer fibrils towards the surface. These rods are probably stiff structures embedded in a soft matrix. It has been shown by shock-freezing experiments in euplantulae of bushcrickets that the fibrillar structure of smooth adhesive pads plays an important role in their ability to conform to rough surfaces (Gorb et al. 2000).

Our study provides some additional morphological details. First, the CLSM images show that the principal fibres are arranged very regularly in longitudinal rows running from the proximal to the distal end of the adhesive contact zone. These rows have a similar spacing as the ridges detected in the AFM height profiles, suggesting that the longitudinal ridges we detected on the surface are determined by the arrangement of the principal rods. Second, the TEM cross-sections show that the fibrous procuticle is covered by an amorphous epicuticle of ca.

250 nm thickness, traversed by thin pore canals. These pore canals may be the route through which adhesive secretion is transported to the surface. Even though we were unable to see these pores in the loose fibrous procuticle (Fig. 3), it is likely that they run from the epidermis to the surface of the epicuticle, as in other types of cuticle (Locke 1961; Gorb 2001). A similar arrangement consisting of a 300 nm deep epicuticle perforated by ~ 10 nm wide pore canals has been reported from the adhesive organs in aphids (Lees and Hardie 1988) and may represent a general feature of smooth adhesive pads in insects. However, the occurrence of pore canals among smooth adhesive pads of insects as well as their ultrastructure is still not sufficiently clear.

The surface height profile recorded by AFM surprisingly depended on the scanning direction of the AFM tip (Fig. 5). It has been hypothesised that, because of the sloped orientation of the principal rods, the pad material is optimised for maximum friction in one direction (Gorb and Scherge 2000). However, friction experiments on the arolium of *C. morosus* did not reveal any direction dependence of the shear stress (force per contact area), indicating that the apparent anisotropy of friction is only based on an increase of contact area when the foot is pulled toward the body (Drechsler and Federle 2005). Even though the friction of whole pads cannot be compared directly with our AFM data, the direction-independence of shear stress seems to be consistent with the absence of a difference between proximal and distal AFM scans in this study. On the other hand, we did observe a significant difference between longitudinal and transverse scans (in either direction). The height of the longitudinal ridges was smaller when the pad was scanned longitudinally. The underlying mechanisms and functional implications of this effect are still unclear. It seems that the pad material is effectively stiffer when it is deformed by a transverse movement and softer during proximal–distal movements. This could have a function for the control of attachment and detachment during locomotion. For example, if transverse movements resulted in a reduced real contact area, they could be used to achieve an easier detachment. Further studies are required to test this possibility.

Mechanical properties

The elastic modulus of the adhesive pad cuticle we found for *C. morosus* is within the range of previous measurements of the softness of smooth adhesive organs in insects (Gorb et al. 2000; Perez Goodwyn et al. 2006). Smooth adhesive pads possess perhaps the softest type of cuticle known among arthropods. Its Young's modulus is comparable to that of sea anemone mesoglea (10 kPa) (Vogel

2003). Being soft is essential for adhesive structures, because they must be deformable to conform to rough surface profiles. According to a criterion coined by Dahlquist (1969), materials are tacky when their elastic modulus (E) is lower than about 10^5 Pa.

An important result of our study is the demonstration that the arolium cuticle consists of layers of different material properties. The AFM force–distance curves show that the arolium cuticle has a softer outer layer of approximately 200 nm thickness. The TEM cross-sections strongly suggest that this layer is the epicuticle. In the TEM images the epicuticle has about the same thickness and similar variation (cf. Figs. 3, 7). The distinctly softer nature of the outermost epicuticle layer could not be detected in previous studies because of the limited spatial resolution of the indentation techniques used. Pad elastic moduli were either estimated from load-displacement curves of entire euplantulae (Gorb et al. 2000; Jiao et al. 2000) or from measurements using spherical indenters with radii and indentation depths >30 μm (Perez Goodwyn et al. 2006). As a consequence, these methods integrated larger volumes of pad material so that the specific properties of the outermost epicuticle and the procuticle could not be differentiated. It is therefore still unclear whether soft outer layers are a general property of smooth adhesive pads of insects.

What are the benefits of having a soft and thin outer layer for an adhesive structure? Creton and Leibler (1996) showed that the Dahlquist criterion holds for rough surfaces and yields a critical modulus E when complete contact between the two surfaces is achieved (even in the absence of an external load). The elastic energy U_{el} necessary to deform a material so that it fills out a substrate cavity of height h and width λ is given by (Persson and Tosatti 2001) $U_{\text{el}} \approx E\lambda h^2$. If this elastic energy is smaller than the gain in adhesion energy $U_{\text{ad}} \approx -\Delta\gamma\lambda^2$, where $\Delta\gamma$ is the change of surface free energy (per unit area) when the material makes contact, then the material will deform spontaneously to fill out the substrate cavities. The condition $U_{\text{el}} = -U_{\text{ad}}$ gives:

$$E = \frac{\Delta\gamma\lambda}{h^2} \quad (8)$$

Thus, a hard material will be able to fill the cavities if $\lambda \gg h$ (i.e. a “smooth” surface), whereas a softer material is required if $\lambda \approx h$ (i.e. a “rough” surface). Many real surfaces are macroscopically smooth (i.e. $\lambda_1 \gg h_1$) but rough on a microscopic length scale (i.e. $\lambda_2 \approx h_2$). As a consequence, a hard material is sufficient to conform to the macroscopic surface profile, but only a soft material will be able to follow the small-scale topography. The amplitude of material deformation caused by small-scale surface topography is of the order $\lambda_2 \approx h_2$.

Thus, even a thin layer of soft material of about this thickness on top of a harder material will be sufficient to achieve complete contact. The macroscopic waviness will be mainly compensated by the underlying harder material.

An analogous, more general argument can be made based on the theoretical analysis of surface roughness and adhesion by Persson and Tosatti (2001), which considers the “self-affine” fractal nature of many real surfaces. Natural surfaces have roughness on a wide range of length scales. The statistical properties of self-affine fractal surfaces do not change for the transformation

$$(x, y) \rightarrow (x\xi, y\xi) \quad z \rightarrow z\xi^H \quad (9)$$

where ξ is a factor representing the “magnification” and (x, y) is a two-dimensional position vector in the surface plane, $0 < H < 1$ and $D_f = 3 - H$ is the fractal dimension. This implies that if h_0 is the amplitude of the surface roughness on the (larger) length scale λ_0 , then the amplitude h of the surface roughness on the smaller length scale λ will be

$$h \approx h_0(\lambda/\lambda_0)^H \quad (10)$$

The condition for adhesion-induced complete contact on the length scale λ (Eq. 8) combined with Eq. 10 gives:

$$E < \frac{A\gamma\lambda_0}{h_0^2} \left(\frac{\lambda_0}{\lambda}\right)^{2H-1} \quad (11)$$

As $\lambda_0/\lambda > 1$, E will rise for decreasing length scales λ if $H > 1/2$. This means that if the material is soft enough to make contact at the larger length scale λ_0 , it will also adhere at all smaller length scales (Persson and Tosatti 2001). However, if $H < 1/2$, E will decrease for smaller length scales λ . This means that, for a piece of homogeneous material, no significant adhesion will be achieved because the material cannot deform sufficiently at small length scales (Persson and Tosatti 2001). If a material of elastic modulus E_0 is able to deform on the larger length scale λ_0 , however, a softer material with a modulus $E < E_0$ may still be able to adhere on a smaller length scale. For even smaller scales, an even softer material will be required etc. As the thickness of the deformation field caused by the surface topography of length scale λ is of the order λ , it is possible to achieve complete contact using a “hard” material (with modulus E_0) covered by layers which become progressively softer and thinner towards the contact surface. Adhesives of this kind would be able to make complete contact even to “anti-adhesive” surfaces where $H < 1/2$, corresponding to fractal dimensions of $D_f > 2.5$.

An alternative strategy for achieving adhesion to such anti-adhesive surfaces would be to use a homogenous, very soft adhesive. However, this would have the disadvantage that because of its thickness and its low modulus, the pad

cuticle would undergo very large strains during detachment and would be more susceptible to wear. An adhesive which is progressively softer towards the surface is more stable and will therefore be less strained during detachment and will be less susceptible to wear.

We propose that the observed pad design in *C. morosus* is an adaptation to achieve adhesion to surfaces where $D_f > 2.5$. Our findings show that the cuticle consists of a stiffer inner and a thin and very soft outer layer. In addition, adhesion on very small length scales may not only be achieved by virtue of the very soft epicuticle but also by the fluid that is secreted into the contact zone of the pad. In fact, it has been demonstrated recently for *C. morosus* that the pad secretion enhances adhesion only to rough substrates but not to smooth surfaces (Drechsler and Federle 2006).

Acknowledgments The authors thank Agnes Weth for excellent technical assistance as well as Patrick Drechsler and Thomas Endlein for the preparation of the TEM samples for Fig. 3. This study was funded by research grants of the Deutsche Forschungsgemeinschaft (SFB 567-TP C6) and the UK Biotechnology and Biological Sciences Research Council.

References

- Arnold JW (1974) Adaptive features on the tarsi of cockroaches (Insecta: dictyoptera). Int J Insect Morphol Embryol 3:317–334
- Attaf M (2004) Connection between the loading curve models in elastoplastic indentation. Mater Lett 58:3491–3498
- Barnes WJP (1999) Tree frogs and tire technology. Tire Technol Int March 99:42–47
- Beutel RG, Gorb SN (2001) Ultrastructure of attachment specializations of hexapods (Arthropoda): evolutionary patterns inferred from a revised ordinal phylogeny. J Zool Syst Evol Res 39:177–207
- Beutel RG, Gorb SN (2006) A revised interpretation of the evolution of attachment structures in hexapods with special emphasis on Mantophasmatodea. Arthropod Syst Phylogeny 64:3–25
- Creton C, Leibler L (1996) How does tack depend on time of contact and contact pressure? J Polym Sci B 34:545–554
- Dahlquist CA (1969) Pressure-sensitive adhesives. In: Patrick RL (eds) Treatise on adhesion and adhesives. vol. 2. Marcel Dekker, New York, pp 219–260
- Drechsler P, Federle W (2005) Adhesion and friction in stick insect tarsal pads. Comp Biochem Physiol A 141:S144
- Drechsler P, Federle W (2006) Biomechanics of smooth adhesive pads in insects: influence of tarsal secretion on attachment performance. J Comp Physiol A 192:1213–1222
- Eisner T, Aneshansley DJ (2000) Defense by foot adhesion in a beetle (*Hemisphaerota cyanea*). Proc Natl Acad Sci USA 97:6568–6573
- Federle W, Rohrseitz K, Hölldobler B (2000) Attachment forces of ants measured with a centrifuge: better “wax-runners” have a poorer attachment to a smooth surface. J Exp Biol 203:505–512
- Federle W, Barnes WJP, Baumgartner W, Drechsler P, Smith JM (2006) Wet but not slippery: boundary friction in tree frog adhesive toe pads. J R Soc Interface 3:689–697
- Gorb S (2001) Attachment devices of insect cuticle. Kluwer, Dordrecht

- Gorb S, Scherge M (2000) Biological microtribology: anisotropy in frictional forces of orthopteran attachment pads reflects the ultrastructure of a highly deformable material. *Proc Biol Soc B* 267:1239–1244
- Gorb S, Jiao Y, Scherge M (2000) Ultrastructural architecture and mechanical properties of attachment pads in *Tettigonia viridissima* (Orthoptera Tettigoniidae). *J Comp Physiol A* 186:821–831
- Jiao Y, Gorb S, Scherge M (2000) Adhesion measured on the attachment pads of *Tettigonia viridissima* (Orthoptera, Insecta). *J Exp Biol* 203:1887–1895
- Holway RT (1935) Preliminary note on the structure of the pretarsus and its possible phylogenetic significance. *Psyche* 43:1–24
- Kendall MD (1970) The anatomy of the tarsi of *Schistocerca gregaria* Forskal. *Z Zellforsch Mikrosk Anat* 109:112–137
- Lees AD, Hardie J (1988) The organs of adhesion in the aphid *Megoura viciae*. *J Exp Biol* 136:209–228
- Locke M (1961) Pore canals and related structures in insect cuticle. *J Biophys Biochem Cytol* 10:589–618
- Malzbender J, de With G, den Toonder J (2000) The P - h^2 relationship in indentation. *J Mater Res* 15:1209–1212
- Morris VJ, Kirby AR, Gunning AP (1999) Atomic force microscopy for biologists. Imperial College Press, London
- Oliver WC, Pharr GM (2004) Measurement of hardness and elastic modulus by instrumented indentation: advances in understanding and refinements to methodology. *J Mater Res* 19:3–20
- Perez Goodwyn P, Peressadko A, Schwarz H, Kastner V, Gorb S (2006) Material structure, stiffness, and adhesion: why attachment pads of the grasshopper (*Tettigonia viridissima*) adhere more strongly than those of the locust (*Locusta migratoria*) (Insecta: Orthoptera). *J Comp Physiol A* 192:1233–1243
- Persson BNJ (2007) Wet adhesion with application to tree frog adhesive toe pads and tires. *J Phys Condens Matter* 19:376110
- Persson BNJ, Tosatti E (2001) The effect of surface roughness on the adhesion of elastic solids. *J Chem Phys* 115:5597–5610
- Reynolds SE (1975) The mechanical properties of the abdominal cuticle of *Rhodnius* larvae. *J Exp Biol* 62:69–80
- Roth LM, Willis ER (1952) Tarsal structure and climbing ability of cockroaches. *J Exp Zool* 119:483–517
- Slifer EH (1950) Vulnerable areas on the surface of the tarsus and pretarsus of the grasshopper (Acrididae, Orthoptera); with special reference to the arolium. *Ann Entomol Soc Am* 43:173–188
- Snodgrass RE (1956) Anatomy of the honey bee. Cornell University Press, Ithaca
- Vincent JF (1981) Morphology and design of the extensible intersegmental membrane of the female migratory locust. *Tissue Cell* 13:831–853
- Vogel S (2003) Comparative biomechanics: life's physical world. Princeton University Press, Princeton and Oxford